Original Research Article: full paper

(2022), «EUREKA: Physics and Engineering»
Number 5

ANALYSIS OF FREQUENCY DEPENDENCE OF COMPLEX IMPEDANCE AND ELECTRICAL CHARACTERIZATION OF Fe_2O_3/KAOLIN CERAMICS FOR CIVIL ENGINEERING APPLICATIONS

Abdeltif Bouchehma✉
Research Laboratory of Physics and Engineers Sciences
Team of Applied Physics and New Technologies[1]
bouchehma@gmail.com

Mohamed Essaleh
Geosciences, Geonvironnement and Civil Engineering Laboratory[2]

Rachid Bouferra
Geosciences, Geonvironnement and Civil Engineering Laboratory[2]

Soufiane Belhouideg
Research Laboratory of Physics and Engineers Sciences
Team of Applied Physics and New Technologies[1]

Mohamed Benjelloun
Geosciences, Geonvironnement and Civil Engineering Laboratory[2]

Imad Sfa
Valorisation of Resources, Environment and Sustainable Development
High National School of Mines of Rabat
ENIM, B. P. 753, Rabat, Morocco, 10100

[1]*Sultan Moulay Slimane university*
FP, Mghila, B.P. 592, Beni Mellal, Morocco, 23000

[2]*Cadi-Ayyad university*
FSTG, B. P. 549, Marrakech, Morocco, 40000

✉**Corresponding author**

Abstract

The complex impedance spectroscopy (CIS) method is usually used in order to analyze the electrical response of different semiconducting disordered materials as a function of frequency at different temperatures. The real and imaginary parts of the complex impedance can show different semicircles in the complex plane that give evidence for the presence of both bulk and grain boundary contributions. Many parameters can be deduced from the analysis of CIS data, such as relaxation times and activation energies. There are some literature data concerning electrical properties of clays and (semiconductor, sand, cement,…)/clay mixtures. Most of the published works are related to the AC conductivity of rocks with the effect of water or oil content but there are no similar studies on the characterization of the microstructure of individual clays as ceramic materials by analyzing their temperature and frequency dependence of their electrical conductivities. Hence, this paper presents an analysis of electric complex impedance of the Fe_2O_3/Kaolin composite in the high temperature range up to 740 °C. Sinusoidal voltage with frequency in the range [100 Hz, 1 MHz] is applied to the material in order to measure the electrical conductivity for various concentrations of Fe_2O_3 from zero to 100 %. The activation energies for the conduction and for the relaxation processes are determined and their dependence on the density of Fe_2O_3 analyzed. Furthermore, let's found that Fe_2O_3 have the effect to increase the electrical conductivity in our samples. From the Nyquist diagrams, only one semi-circle related to the contribution of the grains to the total electrical conduction is identified for all investigated samples.

Keywords: electrical conductivity, semiconductors, kaolin, Fe_2O_3, impedance spectroscopy.

DOI: 10.21303/2461-4262.2022.002312

1. Introduction

Clay minerals are used as clarifiers, adsorption and absorption materials in many industrial applications due to their abundance and low cost [1, 2]. Kaolinites, smectites and micas, are the basic constituents of clay raw materials. They are mainly used in various economic sectors, such as environment, civil engineering, and agriculture [3, 4]. For example, kaolins are considered in the industry of the paint, paper, ceramic, rubber, plastic, and cracking catalyst [5, 6]. The chemical compositions of kaolins obtained from different parts over the world are close to 39.8 % alumina (Al_2O_3), 46.3 % silica (SiO_2) and 13.9 % water [7]. Other elements as iron (Fe_2O_3) and titanium (TiO_2) are present in the industrial kaolin but in small concentrations (of the order of 1 %) and still make a good quality material [8, 9]. In a recent study, authors reported on the influence of elements like SiO_2, Al_2O_3, CaO and MgO in phase transformation of sintered kaolin [10]. Fe_2O_3 modified kaolin was investigated in order to develop a heterogeneous electro-catalytic oxidation of enoxacin [11]. In reference [12], the experimental electrical resistivity data suggest that low-cost raw materials with Fe_2O_3 content should not affect the insulating properties of aluminous porcelain. To our knowledge, very few experimental data of electrical conductivity in the dynamic regime of clay materials were cited in the literature [12–14]. The presence of such metal oxides in ceramic materials can change their electrical behavior causing mainly an increase in their electrical conductivity due to small polaron hopping conduction mechanisms [15]. The goal of this work is to study the influence of the Fe_2O_3 content on the electrical conductivity of pure industrial kaolin by using the useful non destructive experimental technique of impedance spectroscopy (*IS*) [16–18]. This method is largely used to describe the electrical behavior of ceramic materials [12, 14, 19]. It permits to measure the frequency dependence of the real part, Z' and the imaginary part, Z'' of complex impedance Z^* ($Z^* = Z'+jZ''$, where $j^2 = -1$) at a given temperature T. For homogeneous materials, the Z'' versus Z' diagram (Nyquist diagram) is a half circle that can be modelized by a resistance R mounted in parallel with a capacitance C. This capacitance is replaced by the constant phase element (*CPE*) if there is a distribution of relaxation time in the material. In continuation to our previous works on disordered semiconducting materials [20–24], the *IS* characterization will permit us to identify and understand the dominant conduction mechanisms in kaolin in the considered frequency and temperature ranges. For this study, the temperature varies between 25 °C to 750 °C. Below about 300 °C to 400 °C (depending on the concentration of Fe_2O_3), the electrical conductivity of samples is very small. The electric modulus formalism is used in order to identify the predominant microscopic contributions of bulk, grain boundary and electrode polarization effects. To our knowledge, there are no similar experimental data reported for this material in the considered high temperature region. The obtained results permit the investigation of the role of the microstructure of the considered material in the transport properties with the analysis of the influence of the heat treatment on the electrical conductivity. The *IS* data show that kaolin can be considered as a promising low-cost material for commercial use in electronics-related applications when it is mounted in the form of kaolin/glass composite system.

2. Materials and methods

The samples of pure kaolin with Fe_2O_3 as an additive at a various ratios between zero and 100 % of Fe_2O_3 are considered in this work. Kaolin was mixed with Fe_2O_3 until it becomes homogenized and ready to be compressed in form of circular pellets of diameter and thickness in the order of 13 and 2 mm, respectively. Samples were then sintered at 800 °C for 6 h. The chemical composition of the pure kaolin obtained from the X-ray fluorescence spectrometry is given in **Table 1**. The main chemical composition is SiO_2 (55.305 %) and Al_2O_3 (25.754 %) while Fe_2O_3 represent only the composition of 0.381 %.

Table 1

Chemical characteristics of kaolin by X-ray fluorescence spectrometry

Chemical composition (%)	SiO_2	Al_2O_3	Fe_2O_3	MgO	CaO	Na_2O	K_2O	TiO_2	P_2O_5
Kaolin	55.305	25.754	0.381	0.023	0.114	0.094	3.512	0.338	0.015

The phase formation were studied by X-Ray Diffraction (XRD) analysis using a Rigaku SmartLAb diffractometer, with the Bragg-Brentano geometry, using a copper anticathode ($\lambda_{K\alpha} = 1.5406$ Å). The patterns were recorded in the range of 2θ between 5° and 80° with a step of 0.02° and speed of 2°/min (**Fig. 1**). The average crystallite size, D, was calculated from XRD data based on Debye Sherrer's method ($D = K{\cdot}\lambda_{K\alpha}/(\beta_{hkl}\cos(\theta_{hkl}))$) where $K = 0.9$ is a constant and β_{hkl} is the full width half maxima located at any 2θ in the pattern. From the calculations related to the pic located at $2\theta = 28.61°$ in **Fig. 1**, the average crystallite size of the kaolin is found to be 51.2 nm. The density of the considered pure kaolin is calculated to be 1.95 g/cm^3. The microstructure of the sintered pellets were detected by Scanning Electron Microscopy (SEM) using TESCAN VEGA3 with beam energy of 10 kV coupled with the chemical microanalysis of energy dispersive X-ray spectrometry (EDX) (**Fig. 2, *a*** for the pure kaolin and **Fig. 2, *b*** for the pure kaolin mixed with 20 % of Fe_2O_3 (as example)). According to the SEM and EDX analysis, the kaolin show a porous crystalline structure composed mainly of kaolinite, that is to say aluminum silicates with a chemical formula Al_2SiO_5.

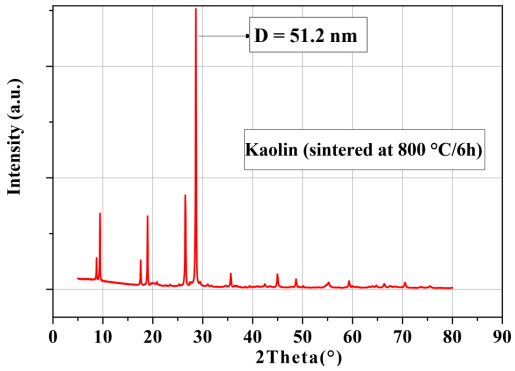

Fig. 1. The X-ray diffractomer of the sintered pure kaolin at 800 °C/6 h used

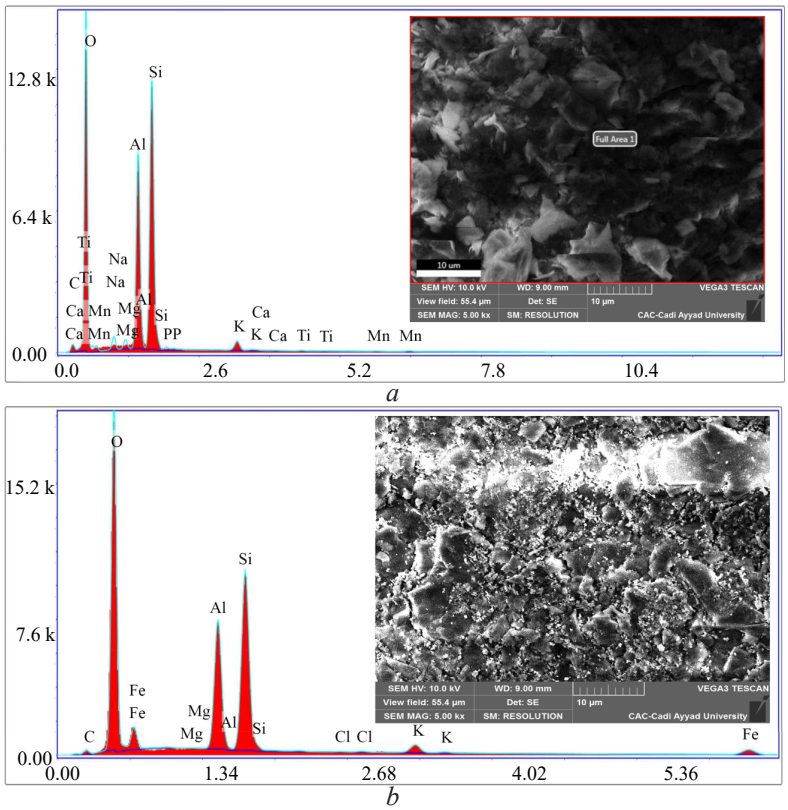

Fig. 2. EDX and SEM images of the:
a – sintered pellet pure kaolin; *b* – sintered pellet kaolin mixed with 20 % of Fe_2O_3

The presence of kaolinite is also confirmed by the band at around 3689 cm^{-1} [25] in the infrared spectrum of the kaolin (not shown here). Finally, the *AC* electrical measurements were done by an HP4284A system in a frequency range from 100 Hz to 1 MHz with an applied voltage of 500 mV. Pellets of 13 mm in diameter and 2 mm in thickness using 0.6 g of Fe_2O_3/kaolin composite were prepared by uniaxial pressing of 5 MPa and covered with silver electrodes.

3. Results and discussion

It is well known that the complex impedance (Z^*) and the electric modulus (M^*) formalisms are usually used to identify and distinguish the contribution of largest resistance from those of smallest capacitance. According to the classical theory of Debye [16], Z^* is given by:

$$Z^* = Z' + jZ'', \text{ where } Z' = \frac{R}{1+(\omega\tau)^2}, \text{ and } Z'' = -R\left(\frac{\omega\tau}{1+(\omega\tau)^2}\right), \quad (1)$$

and M^*, by

$$M^* = j\omega C_o Z^* = M' + jM'', \text{ where } M' = \frac{C_o}{C}\left(\frac{(\omega\tau)^2}{1+(\omega\tau)^2}\right), \text{ and } M'' = \frac{C_o}{C}\left(\frac{\omega\tau}{1+(\omega\tau)^2}\right). \quad (2)$$

In these expressions, C_o is the capacitance of the empty cell while R and C represent the resistance and the capacitance of the material. The relaxation time τ satisfies the condition $2\pi f_0\tau = 1$, where f_o is the frequency at which the curve Z'' versus frequency presents a minimum. This minimum must correspond to a maximum in M''. Nyquist presentation (Z'' versus Z') and (M'' versus M') are the most common methods used to visualize and identify different contributions in a given temperature and frequency ranges.

Fig. 3 illustrates the evolution of the electrical resistivity as a function of the inverse of temperature ($1/T$) at a given frequency of 1 kHz and for various concentrations of Fe_2O_3 (0, 20, 40, 60, 80, 90 and 100 %). In the high temperature from 500 to 740 °C, from the slopes of the obtained straight lines, the activation energy for the conduction process E_{cond}, via the equation:

$$\rho = \rho_0 \exp\left(\frac{E_{cond}}{k_B T}\right), \quad (3)$$

where ρ_o is a pre-exponential factor, T is the absolute temperature and k_B is the Boltzmann constant, is determined for all investigated samples. E_{cond} increases (see the inset of **Fig. 3**) with the increase of the concentration of Fe_2O_3 from 754 meV for pure kaolin to 1028 meV for pure Fe_2O_3. As it is possible to see from **Fig. 3**, the effect of Fe_2O_3 is to increase the electrical conductivity of the system over the considered range of temperature up to 740 °C. For temperatures lower than 400 °C, the local activation energy for the conduction process becomes very small and the electrical conductivity is practically temperature independent indicating the insulating behavior of the material in this domain of temperature. In **Fig. 4**, the electrical conductivity (σ) of the mixed kaolin with Fe_2O_3 is plotted against frequency for a given temperature of 700 °C. σ increases with frequency and also, as mentioned before, with the concentration of Fe_2O_3. The plateau region (low frequency domain) corresponding to dc conductivity (σ_{dc}) is found to extend to higher frequencies when the percentage of Fe_2O_3 increases. The frequency at which the dispersion takes place, also known as hopping frequency, increases with increasing of the % Fe_2O_3. This behavior suggests that electrical conductivity occurs via hopping mechanism, which is governed by the Jonscher universal power law ($\sigma = \sigma_{dc} + A\omega^s$) where A is the pre-exponential factor and s is the fractional exponent between 0 and 1.

Fig. 5 shows the variation of the imaginary part (Z'') of the complex impedance with frequency for various temperatures and for some representative samples (0, 40, 60 and 100 % of Fe_2O_3). Only one single peak is observed at certain frequency ($f_o = f_o(T)$) suggesting the existence of a single contribution (grains, grain boundaries or electrodes) in all samples. These peaks shift towards high frequencies when the temperature increases, indicating the relaxation behavior of the material. Also, a peak broadening is noticed with increasing temperature, which suggests the presence of a distribution of relaxation times in our samples.

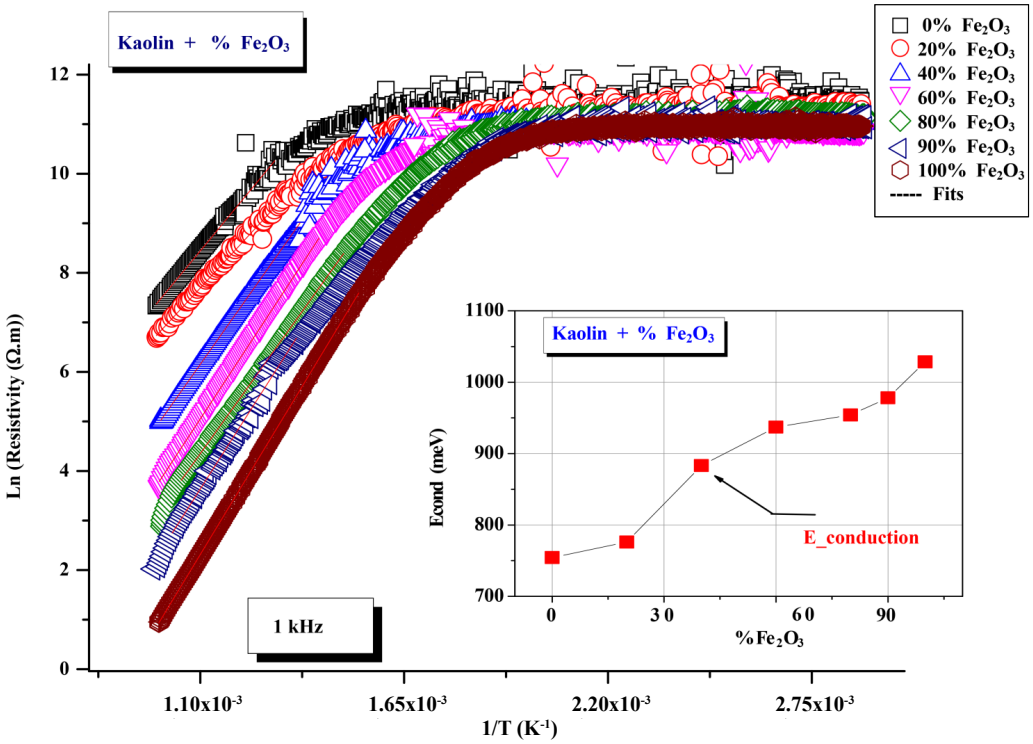

Fig. 3. Variation of the electrical resistivity of the kaolin mixed with Fe_2O_3 as a function of inverse of temperature ($1/T$) with the corresponding activation energies for the conduction process (E_{cond})

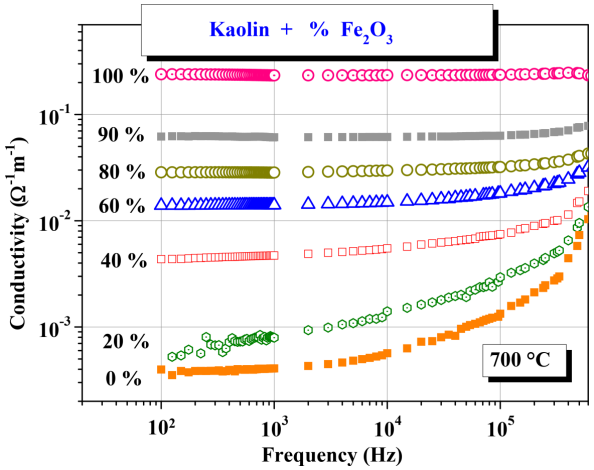

Fig. 4. Variation of the electrical conductivity of the mixed kaolin with Fe_2O_3 as a function of frequency at a given temperature of 700 °C

In **Fig. 6**, the relaxation time (τ) which is calculated from the condition $2\pi f_o \tau = 1$, is plotted against $1/T$. Linear behavior is observed for all samples in the considered temperature range up to 740 °C. From the corresponding slopes, the activation energy for the relaxation process (E_{relax}) is deduced by considering the equation $\tau = \tau_0 \exp(-E_{relax}/k_B T)$, where τ_0 is the relaxation time at infinite temperature. E_{relax} increases (see the inset of **Fig. 6**) with the increase of the concentration of Fe_2O_3 from 904 meV for pure kaolin to 1129 meV for pure Fe_2O_3.

As it is also possible to see from **Fig. 6**, the effect of Fe_2O_3 is to decrease the relaxation time of the system.

A comparison between E_{cond} and E_{relax} is given in **Fig. 7**. Let's conclude that E_{cond} is always lower than E_{relax}.

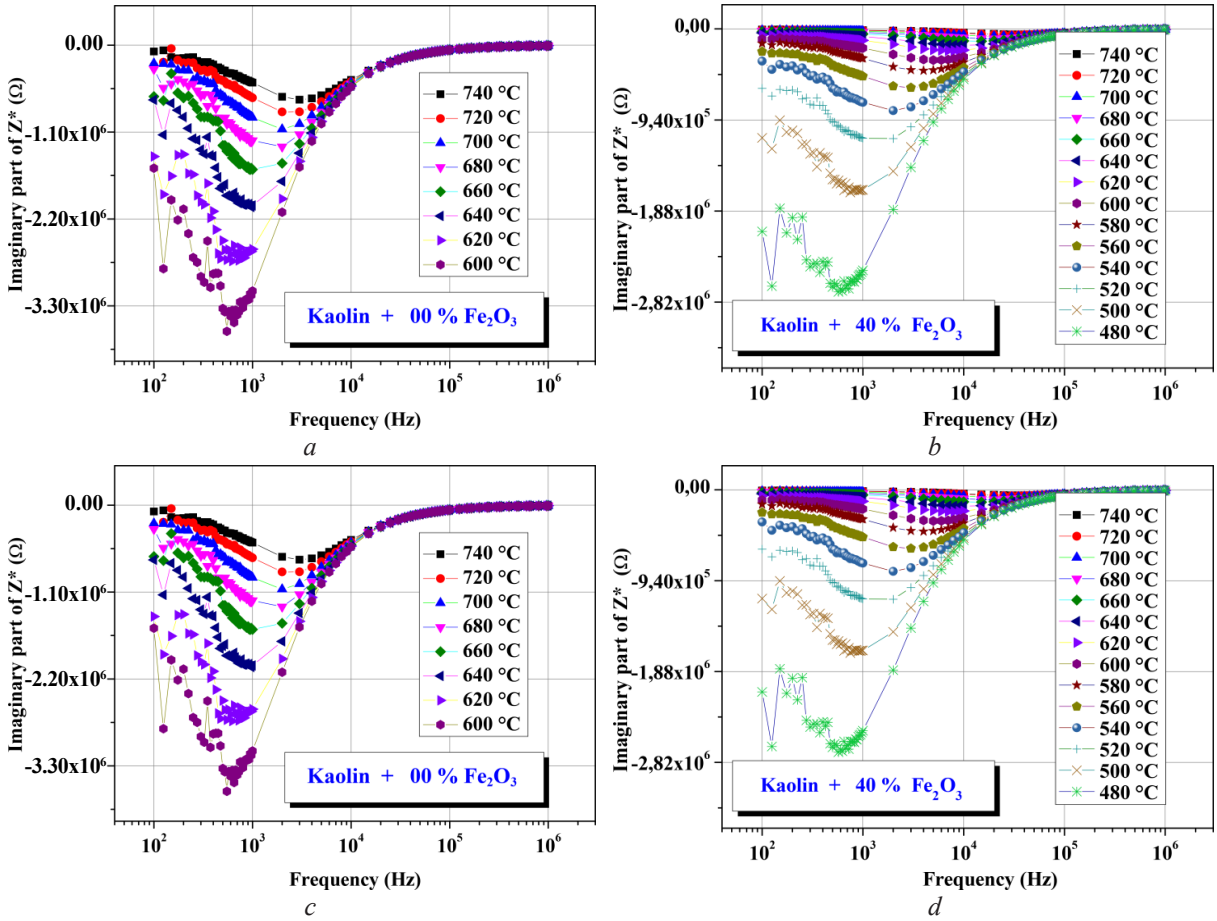

Fig. 5. Variation of imaginary part of complex impedance of the mixed kaolin with *x* % of Fe_2O_3 as a function of frequency: *a* – 0 %; *b* – 40 %; *c* – 60 %; *d* – 100 %

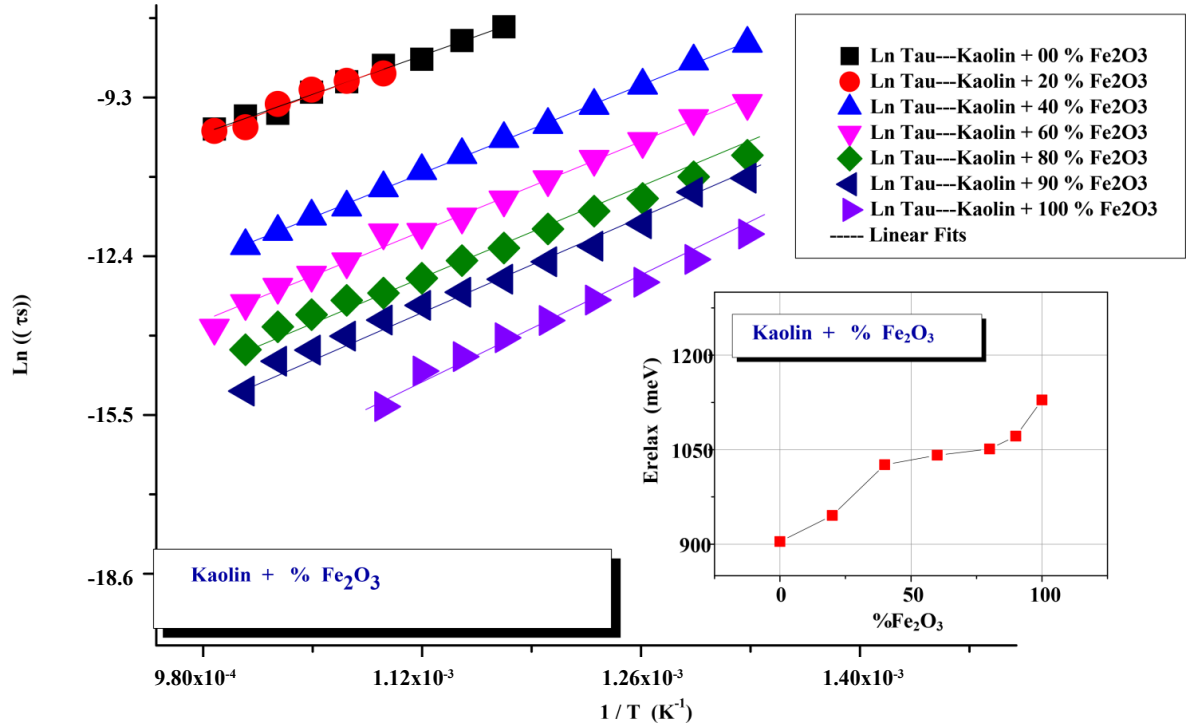

Fig. 6. Arrhenius plots of relaxation time for all samples

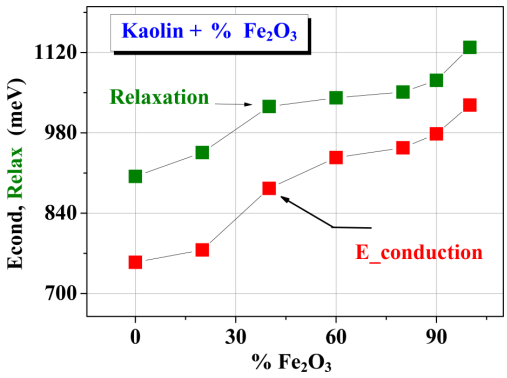

Fig. 7. Comparison between the activation energies for the conduction (E_{cond}) and for the relaxation (E_{relax}) processes for all samples

In **Fig. 8**, for a given temperature of 700 °C, a single semicircle, which is attributed to the contribution of the grains, is observed in the investigated samples. The diameter of the semicircle decreases with the increase of the concentration of Fe_2O_3 indicating the increase in the electrical conductivity. In relation with the distribution of the relaxation time, as mentioned before, an equivalent electrical circuit consisting of a resistor (R) mounted in parallel with a constant phase element (CPE) can be considered in order to describe the impedance spectra of our samples.

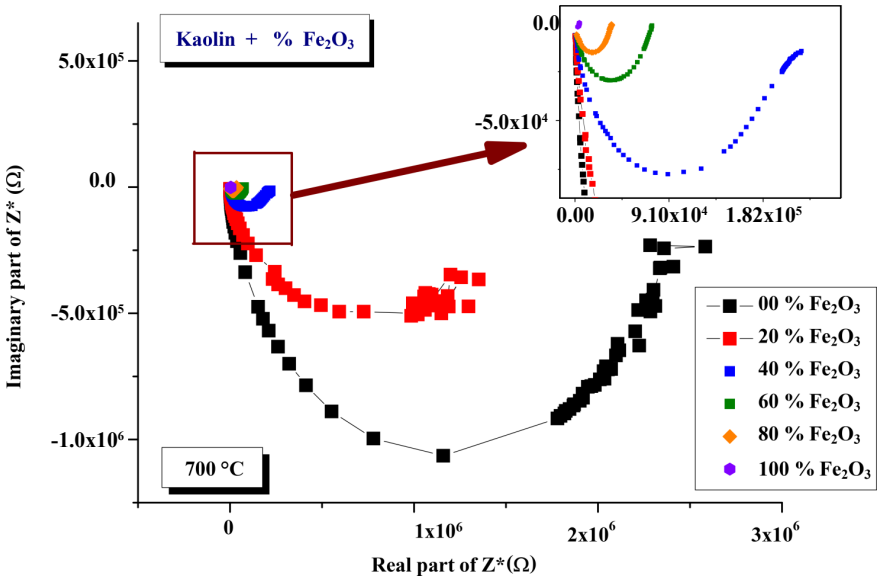

Fig. 8. Imaginary (Z'') versus real (Z') parts of the complex impedance (Z^*) for all samples at a given temperature of 700 °C

In this case, Z' and Z'' are given by the following expressions:

$$Z' = \frac{R\left(1 + RQ\omega^n \cos\left(\frac{n\pi}{2}\right)\right)}{1 + 2RQ\omega^n \cos\left(\frac{n\pi}{2}\right) + \left(RQ\omega^n\right)^2}; \; Z'' = \frac{R^2 Q\omega^n \sin\left(\frac{n\pi}{2}\right)}{1 + 2RQ\omega^n \cos\left(\frac{n\pi}{2}\right) + \left(RQ\omega^n\right)^2}, \tag{4}$$

where the impedance of the constant phase element (CPE) is $Z_{CPE} = 1/Q(j\omega)^n$. In these equations, Q is a constant which is independent of frequency. The exponent n measures the degree of distortion of Z'' vs. Z'. The value of n is equal to 1 for an ideal capacitor. From the best fit of the data of **Fig. 8** by the electric circuit of R mounted in parallel with CPE is shown in **Fig. 8**, the values of the adjustable parameters R, Q, and n used in these fits are given in **Table 2**.

Table 2

Values of the adjustable parameters *R*, *Q*, and *n* used in the fits of the data with an equivalent circuit

Sample	*R* (Ω)	*Q*	*n*	*C*(*F*)
00 % Fe_2O_3	$2.3873 \cdot 10^6$	$5.828 \cdot 10^{-11}$	0.94312	$3.41136 \cdot 10^{-11}$
20 % Fe_2O_3	$1.2986 \cdot 10^6$	$1.26 \cdot 10^{-10}$	0.8917	$4.37048 \cdot 10^{-11}$
40 % Fe_2O_3	189950	$1.022 \cdot 10^{-10}$	0.9089	$3.44486 \cdot 10^{-11}$
60 % Fe_2O_3	71621	$1.333 \cdot 10^{-10}$	0.89191	$3.28431 \cdot 10^{-11}$
80 % Fe_2O_3	34459	$9.386 \cdot 10^{-11}$	0.91778	$3.02437 \cdot 10^{-11}$
100 % Fe_2O_3	4298	$3.973 \cdot 10^{-11}$	0.97769	$2.78412 \cdot 10^{-11}$

The corresponding capacitance $C = \left(R^{1-n}Q\right)^{1/n}$, at 700 °C is calculated to be of the order of 10^{-11} F, a typical known value for the grains in disordered materials.

During a heat treatment of kaolin, this material undergoes physico-chemical transformations which lead to both a modification of its crystalline structure of the different phases and a modification of its microstructure. The development of the ceramic industry requires raw materials with low density of impurities. Indeed the presence of these impurities influences the densification and porosity. These physico-chemical characteristics play an important role in the mechanical, colorimetric and electrical properties. The electrical properties of our kaolin seem interesting because they are in the field of insulating ceramics despite the presence of iron in large quantities. All the obtained results can be applied in the field of traditional ceramics industry but also technical ceramics where attention must be paid to iron, which was known, but also to titanium to avoid the formation of secondary porosity at high temperature.

4. Conclusions

Fe_2O_3/Kaolin ceramics with different concentrations of Fe_2O_3 were prepared by mixing pure kaolin powder and Fe_2O_3. The ceramics were sintered at 800 °C during 6 h. Their structural and morphological properties have been discussed. The electrical conduction is thermally activated and depends on the concentration of Fe_2O_3. The activation energies for the conduction and for the relaxation processes are determined for all samples. E_{relax} and E_{cond} increase with the increase of the concentration of Fe_2O_3 with E_{cond} always lower than E_{relax}. The impedance results prove the predominance of only one contribution of the grains to the electrical conductivity in all investigated samples. The experimental data of the complex impedance can be analyzed by an equivalent electrical circuit consisting of a resistor (*R*) mounted in parallel with a constant phase element (*CPE*).

Conflict of interest

The authors declare that there is no conflict of interest in relation to this paper, as well as the published research results, including the financial aspects of conducting the research, obtaining and using its results, as well as any non-financial personal relationships.

References

[1] Murray, H. H. (1999). Applied clay mineralogy today and tomorrow. Clay Minerals, 34, 39–49. doi: http://doi.org/10.1180/000985599546055

[2] Bergaya, F., Lagaly, G.; Bergaya, F. et. al. (Eds.) (2006). Clays, Clay Minerals, and Clay Science, Developments in Clay Science. Handbook of clay science. Amsterdam: Elsevier. doi: http://doi.org/10.1016/s1572-4352(05)01001-9

[3] Konta, J. (1995). Clay and man: clay raw materials in the service of man. Applied Clay Science, 10 (4), 275–335. doi: http://doi.org/10.1016/0169-1317(95)00029-4

[4] Harvey, C. C., Murray, H. H. (1997). Industrial clays in the 21st century: A perspective of exploration, technology and utilization. Applied Clay Science, 11 (5-6), 285–310. doi: https://doi.org/10.1016/S0169-1317(96)00028-2

[5] Wei, L., Zhongyi, F., Jun, W., Qing, H., Hang, D., Xiaojuan, Z., Zhi, Z. (2021). Study on the reusability of kaolin as catalysts for catalytic pyrolysis of low-density polyethylene. Fuel, 302, 121164. doi: https://doi.org/10.1016/j.fuel.2021.121164

[6] Xinbin, L., Xiaoyang, X., Weihui, J., Jian, L., Lifeng, M., Qian, W. (2020). Influences of impurities and mineralogical structure of different kaolin minerals on thermal properties of cordierite ceramics for high-temperature thermal storage. Applied Clay Science, 187, 105485. doi: https://doi.org/10.1016/j.clay.2020.105485

[7] Murray, H. H. (1991). Overview – clay mineral applications. Applied Clay Science, 5 (5-6), 379–395. doi: https://doi.org/10.1016/0169-1317(91)90014-Z

[8] Ababneh, A., Matalkah, F., Matalkeh, B. (2002). Effects of kaolin characteristics on the mechanical properties of alkali-activated binders. Construction and Building Materials, 318, 126020. doi: https://doi.org/10.1016/j.conbuildmat.2021.126020

[9] Vesely, D. Kalendova A., Victor Manso, M. (2012). Properties of calcined kaolins in anticorrosion paints depending on PVC, chemical composition and shape of particles. Progress in Organic Coatings, 74 (1), 82–91. doi: https://doi.org/10.1016/j.porgcoat.2011.11.017

[10] Jamil, N. H., Abdullah, M. M. AB., Pa, F. C., Mohamad, H., Ibrahim, W. M., Chaiprapa, J. (2020). Influences of SiO_2, Al_2O_3, CaO and MgO in phase transformation of sintered kaolin-ground granulated blast furnace slag geopolymer. Journal of Materials Research and Technology, 9 (6), 14922–14932. doi: https://doi.org/10.1016/j.jmrt.2020.10.045

[11] Özcan, A., Özcan, A. A., Demirci, Y., Şener, E. (2017). Preparation of Fe2O3 modified kaolin and application in heterogeneous electro-catalytic oxidation of enoxacin. Applied Catalysis B: Environmenta, 200, 361–371. doi: https://doi.org/10.1016/j.apcatb.2016.07.018

[12] Piva, D. H., Piva, J., Venturini, J., Ramon, J., Caldas, V., Morelli, M. R., Bergmann, C. P. (2016). Effect of Fe_2O_3 content on the electrical resistivity of aluminous porcelain applied to electrical insulators. Ceramics International, 42 (4) 5045–5052. doi: https://doi.org/10.1016/j.ceramint.2015.12.016

[13] de Lima, O. A. L., Sharma, M. N. (1992). A generalized Maxwell-Wagner theory for membrane polarization in shaly sands. Geophys, 57 (3), 431. doi: https://doi.org/10.1190/1.1443257

[14] Piva, R. H. Vilarinho, P. MorelliM, M. R. Fiori, M. A. Montedo, O. R. K. (2013). Influence of Fe_2O_3 content on the dielectric behavior of aluminous porcelain insulators. Ceramics International, 39 (7), 7323–7330. doi: https://doi.org/10.1016/j.ceramint.2013.02.071

[15] Bosman, A. J., Van Daal, H. J. (1970). Small-polaron versus band conduction in some transition-metal oxides. Advances in Physics, 19 (77), 1–117. doi: https://doi.org/10.1080/00018737000101071

[16] Barsoukov, E., Macdonald, J. R. (2005). Impedance Spectroscopy: Theory, Experiment, and Applications. New York: Wiley. doi: https://doi.org/10.1002/0471716243

[17] Elliot S. R. (1987). Temperature dependence of a.c. conductivity of chalcogenide glasses. Philosophical Magazine B, 37 (5), 553–560. doi: https://doi.org/10.1080/01418637808226448

[18] Jonscher, A. K. (1992). Dielectric Relaxation in Solids. Journal of Physics D: Applied Physics, 32 (14), 57–70. doi: http://doi.org/10.1088/0022-3727/32/14/201

[19] Bona, N., Rossi, E., Capaccioli, S. (2001). Electrical Measurements in the 100 Hz to 10 GHz Frequency Range for Efficient Rock Wettability Determination. SPE Journal 6 (01), 80–88. doi: https://doi.org/10.2118/69741-PA

[20] Bouchehma, A., Essaleh, L., Marín, G., Essaleh, M., Wasim, S. M., Amhil, S. et. al. (2021). Physica B: Dielectric spectroscopy of *n* type $Cu_5In_9Se_{16}$ semiconductor compound, Condensed Matter, 622, 413356. doi: https://doi.org/10.1016/j.physb.2021.413356

[21] Bouferra, R., Marín, G., Amhil, S., Wasim, S., Essaleh, L. et. al. (2020). Electrical impedance spectroscopy characterization of *n* type $Cu_5In_9Se_{16}$ semiconductor compound, Physica B: Condensed Matter, 593. doi: https://doi.org/10.1016/j.physb.2020.412283

[22] Essaleh, L., Wasim, S. M., Marın, G., Rincon, C., Amhil, S., Galibert, J. (2017). Mott type variable range hopping conduction and magnetoresistance in p-type $CuIn_3Te_5$ semiconductor compound. Journal of Applied Physics 122. 015702. doi: https://doi.org/10.1063/1.4991004

[23] Essaleh, L., Amhil, S., Wasim, S. M., Marín, G., Choukri, E. (2018). Theoretical and experimental study of AC electrical conduction mechanism in the low temperature range of p-$CuIn_3Se_5$. Physica E Low-dimensional Systems and Nanostructures, 99, 37–42. doi: https://doi.org/10.1016/j.physe.2018.01.012

[24] Kirou, H., Atourkia, L., Essaleh, L., Taleb, A., Messous, M. Y., Bouabid, K., Nya, N., Ihlal, A. (2019). Towards phase pure Kesterite Cu_2ZnSnS_4 thin films via Cu-Zn-Sn electrodeposition under a variable applied potential. Journal of Alloys and Compounds, 783, 524–532. doi: https://doi.org/10.1016/j.jallcom.2018.12.269

[25] Janek, M., Zich, D., Naftaly, M. (2014). Terahertz time-domain spectroscopy response of amines and amino acids intercalated smectites in far-infrared region. Materials Chemistry and Physics, 145, 278–287. doi: https://doi.org/10.1016/j.matchemphys.2014.02.004

Received date 14.03.2022
Accepted date 20.07.2022
Published date 30.09.2022

How to cite: *Bouchehma, A., Essaleh, M., Bouferra, R., Belhouideg, S., Benjelloun, M., Sfa, I. (2022). Analysis of frequency dependence of complex impedance and electrical characterization of Fe_2O_3/kaolin ceramics for civil engineering applications. EUREKA: Physics and Engineering, 5, 175–183. doi: https://doi.org/10.21303/2461-4262.2022.002312*